1 × *N* star coupler as a distributed fiber-optic strain sensor in a white-light interferometer

Libo Yuan and Limin Zhou

A novel technique of using a $1 \times N$ star fiber optic coupler as a distributed strain sensor in a white-light interferometer to measure the distribution of strain is presented. The measuring principle and 1×4 star coupler with four fiber optic strain sensors are demonstrated. The experiment is performed with four sensors attached to a combination plastic specimen. © 1998 Optical Society of America

  OCIS codes: 060.2370, 060.1810, 120.3180.

1. Introduction

White-light interferometry as a technique that employs low-coherence, broadband sources has been an active research area in recent years.[1–8] The main advantages of this technique lie in its ability to facilitate absolute measurements, such as position and displacement, with high resolution.[9,10] A distributed fiber optic strain-sensing system based on Michelson white-light interferometer, in which a $1 \times N$ fiber optic star coupler plays the role of distributed sensor, has been developed and is demonstrated. It is suitable for measuring the distribution strain in smart materials and structures.

2. Distribution Sensing System

The fiber optic Michelson interferometer is a well-established and widely used technique. Two light beams are reflected and recombined in a Michelson configuration. When the optical-path difference between the two beams falls within the coherence length of the source, a white-light fringe pattern is produced, and the central fringe, which is located in the center of the fringe pattern and has the highest amplitude, corresponds to the exact optical-path match of the two beams.[11] The transfer function of

a two-beam interferometer illuminated by partially coherent light is described as

$$I(x) = I_{\text{mean}}\left[1 + \exp\left(-\frac{\xi^2}{2L_c^2}x^2\right)\cos\left(\frac{2\pi}{\lambda_0}x\right)\right], \quad (1)$$

where I_{mean} is the average intensity of the interferometer output, x is the optical-path difference introduced by the interferometer, ξ is the spectrum coefficient of the LED itself, and $L_c = \lambda_0^2/\Delta\lambda$ is the coherence length of the source. Here λ_0 is the central wavelength of the spectrum and $\Delta\lambda$ is the full width at half-maximum of the spectrum of the light source.

Using the principle discussed above, we designed a distributed strain-sensing system in which a $1 \times N$ fiber optic star coupler is used as N distributed strain sensors. A schematic of the distribution sensing system is illustrated in Fig. 1.

The light from a 1300-nm LED is split by a 3-dB 2×2 single-mode coupler into two beams, configuring a Michelson interferometer. One of the two branches of the interferometer is connected with a $1 \times N$ star coupler, in which the N arms' fiber ends are polished and coated with reflectivity R. Each of the N fiber arms of the $1 \times N$ star coupler acts as one strain sensor; then the N different-length arms form N distribution strain sensors. The other branch is connected to a finite-length fiber as a balance measuring arm and terminates with a gradient-index (GRIN) lens and is perpendicular to a reflective mirror. The mirror mounted upon a motor-driven linear positioning stage is used for scanning each reflective end surface of the N fiber optic sensors, which can match the absolute elongation of each sensing fiber length.

  L. Yuan is with the Department of Physics, Harbin Engineering University, Harbin 150001, China. L. Zhou is with the Department of Mechanical Engineering, The Hong Kong Polytechnic University, Hong Kong, China.

Fig. 1. Distribution fiber optic strain-sensing system: PIN, detector; FC's, fiber connector.

(a) Transverse distribution strain measuring of the bulk structure.

(b) Longitude distribution strain measuring of the bulk structure.

Fig. 3. Two principal methods for embedding fiber optic sensors.

3. Measuring Principle

Figure 2 is a schematic of the measuring principle of the fiber optic distribution sensing system. In Fig. 2 the lengths of the N arms of the $1 \times N$ star coupler are equal to $l_1, l_2, \ldots, l_N$, as N sensors. Assume that l_1 changes to $l_1 + \Delta l_1$, l_2 changes to $l_2 + \Delta l_2, \ldots,$ l_N changes to $l_N + \Delta l_N$, as distributed stresses are loaded in the fiber sensing gauges. Then the distribution strains are $\varepsilon(1) = \Delta l_1/l_1$, $\varepsilon(2) = \Delta l_2/l_2, \ldots,$ $\varepsilon(N) = \Delta l_N/l_N$, where l_i $(i = 1, 2, \ldots, N)$ is the embedded gauge length of the sensing optical fiber arms. To avoid the confusion in measuring, the lengths of the fiber sensors can be

$$l_1 < l_2 < \cdots < l_N \qquad (2)$$

and the differential length of the two fiber sensors should be satisfied:

$$n_{\text{eff}}(l_{i+1} - l_i)_{\min} > n_{\text{eff}}\varepsilon_{\max}l_{i+1} + L_c, \qquad i = 1, 2, \ldots, N - 1 \qquad (3)$$
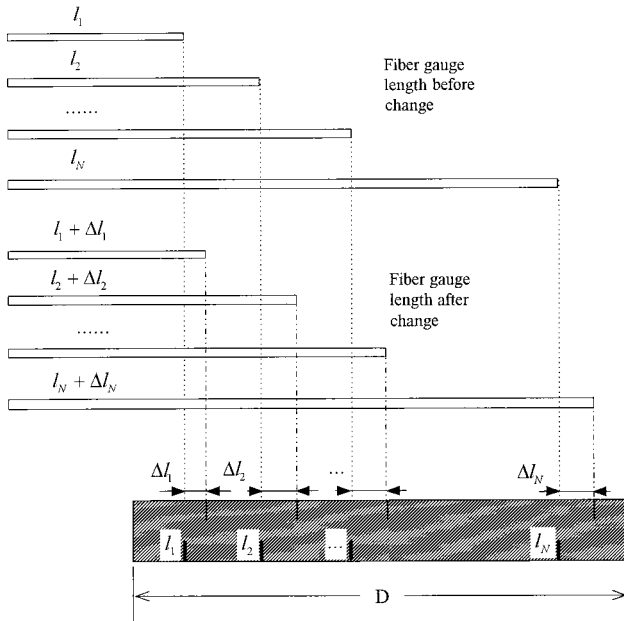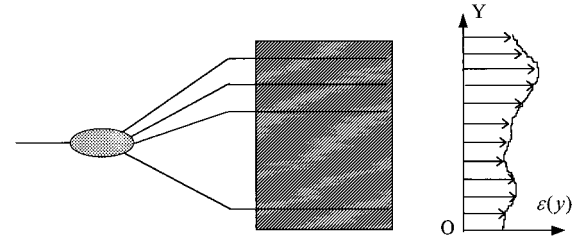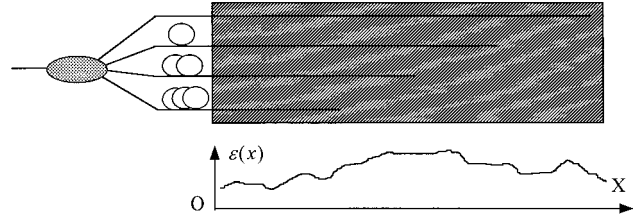

Fig. 2. Measuring principle of the fiber-optic distribution sensing system.

to avoid cross sensitivity among the N measurement channels. In practice, the differential length of each of the two fiber sensors is measured in millimeters. Here n_{eff} is the effective refractive index of the fiber core and $\varepsilon_{\max}$ represents the maximum strain of all fiber optic sensors.

To ensure that each fiber sensor is within the scanning measuring range, the differential of the shortest and the longest fiber sensors should be satisfied:

$$n_{\text{eff}}(l_N - l_1)_{\max} < D, \qquad (4)$$

where D is the longest motor stage scanning distance. The two principal methods for measuring the distribution strain of the structure with embedded fiber optic sensors are sketched in Fig. 3.

4. Calculation of Light Power

For the fiber optic sensing system, assume that the light power from the LED source launched into the fiber is P_0 and is split by a 3-dB single-mode coupler into two parts. In the sensing branch the light power is $P_0/2$. When it encounters a connector and then is divided into N parts by the $1 \times N$ star coupler, the power of the transmission light in each arm can be calculated as

$$P_T(i) = \frac{P_0}{2}\delta_c\alpha_s T_i, \qquad i = 1, 2, \cdots, N, \qquad (5)$$

where δ_c is the parameter of the connector insertion losses, defined as

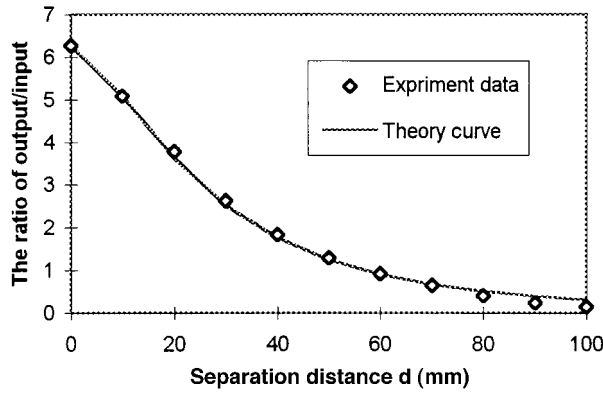$$\delta_c = \frac{P_{\text{output}}}{P_{\text{input}}}, \qquad (6)$$

Fig. 4. Typical single-mode fiber GRIN lens collimator insertion losses versus separation distance.

α_s is the star coupler insertion loss, defined as

$$\alpha_s = \frac{\sum_i^N P_{i(\text{output})}}{P_{(\text{input})}}, \qquad (7)$$

and T_i is the ratio of the light power, described by

$$T_i = \frac{P_{i(\text{output})}}{\sum_j^N P_{j(\text{output})}}, \qquad i = 1, 2, \cdots, N. \qquad (8)$$

If the $1 \times N$ star coupler's output port is uniform, Eq. (8) becomes

$$T_i = \frac{1}{N}, \qquad i = 1, 2, \cdots, N. \qquad (9)$$

Thus the reflected light power received by the detector can be given by

$$P_R(i) = P_0 \left(\frac{\delta_c \alpha_s T_i}{2} \right)^2 R_i = P_0 \left(\frac{\delta_c \alpha_s}{2N} \right)^2 R_i, i = 1, 2, \cdots, N. \qquad (10)$$

Here R_i is the reflectivity of the end the ith sensing arm.

Similarly, the light power reflected from the measuring arm is estimated as

$$P_s = P_0 \left(\frac{\delta_c}{2} \right)^2 \eta(d) R_s, \qquad (11)$$

where R_s is the reflectivity of the mirror and $\eta(d)$ represents the insertion losses of the GRIN lens collimator determined by experiment, as shown in Fig. 4. According to the testing data, these losses can be approximately described as

$$\eta(d) = \frac{A}{[1 + \xi(d/r_0)^{3/2}]^2}, \qquad (12)$$

where d is the distance between the end of GRIN lens and the mirror and $r_0 = 1.5$ mm is the radius of the GRIN lens. For the GRIN lens collimator in our

Table 1. Parameters of the Experimental System

Quantity	Symbol	Value	Unit
Connector insertion loss	δ_c	0.3	dB
1×4 Star coupler insertion loss	α_s	0.2	dB
Arm 1 splitting ratio of star coupler	T_1	16.5	%
Arm 2 splitting ratio of star coupler	T_2	17.6	%
Arm 3 splitting ratio of star coupler	T_3	13.2	%
Arm 4 splitting ratio of star coupler	T_4	52.7	%
Reflectivity of sensing arm fiber end	$R_i \ (i = 1\text{--}4)$	91.5	%
Reflectivity of mirror	R_s	94.7	%

experiment the dimensionless parameters are $A = 6.266$ and $\xi = 0.0065$.

The upper limit of the sensor number can be estimated from Eq. (10). We assume that the minimum optical power is 50 nW to ensure the identification of the white-light interference pattern's central fringe and neglect the insertion losses caused by the connector and the coupler; then $N \approx 7$ for $R_1 = 100\%$ and $P_0 = 10 \ \mu$W and $N \approx 22$ if $P_0 = 100 \ \mu$W. We used a 1300-nm LED with $\Delta\lambda = 43$ nm as a white-light source; the optical power launched into the single-mode fiber was 11.08 μW with drive current 50 mA, and a 1×4 single-mode star coupler at wavelength of 1300 nm was used as four distribution sensors. The relevant parameters are listed in Table 1.

5. Testing Results

A schematic of the testing arrangement is shown in Fig. 5. Single-mode fibers with 9–125-μm core–cladding diameters and 35-μm-thick polymer coatings were used in the experiment. The gauge length of the four sensing fibers was 250 mm, and the fibers were attached with epoxy to a three-layer combination plastic plate. The strain was uniform for each part of the combination plate. By the side of the fiber we used an electrical resistance strain gauge to calibrate the fiber optic sensor.
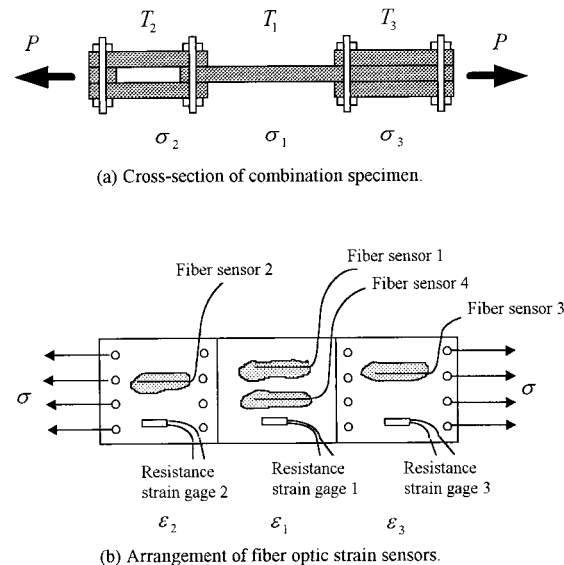

(a) Cross-section of combination specimen.

(b) Arrangement of fiber optic strain sensors.

Fig. 5. Three-layer combination plastic strain-testing specimen.

The fiber optic sensor's lengths change as force P is applied to the two ends of the combination plastic plate. For sensor 1, for instance, working in the unloaded state, the mirror scans a short distance in front of the measuring arm (see Fig. 1). Once the sum of the scanned distance plus the length of the measuring arm equals that of the sensing arm, white-light fringes appear. The zero-order fringe, which is approximately in the center of fringe pattern and has the highest amplitude, corresponds to the exact optical-path match of these two beams. Thus the initial position will be recorded as the reference position when this procedure is repeated and a new white-light fringe pattern will be established because of straining of the sensing arm. As shown in Fig. 2, the distance between the zero-order fringe patterns for the unchanged initial position and the deformed position gives the amount of optical-path difference Δx, which can be expressed as

$$\Delta x = n\Delta l(\varepsilon) + \Delta n(\varepsilon)l, \qquad (13)$$

where l is the fiber optic sensor gauge length. The first term in Eq. (13) represents the physical change in length produced by the strain, which is directly related to axial strain ε through the expression

$$\Delta l(\varepsilon) = l\varepsilon. \qquad (14)$$

The second term, the change in optical path that is due to a change in the refractive index of the fiber core, it is given by[12]

$$\Delta n = -1/2n^3[(1-\mu)p_{12} - \mu p_{11}]\varepsilon. \qquad (15)$$

Thus we have

$$\Delta x = nl\varepsilon - 1/2n^3[(1-\mu)p_{12} - \mu p_{11}]l\varepsilon$$
$$= \{n - 1/2n^3[(1-\mu)p_{12} - \mu p_{11}]\}l\varepsilon$$
$$= n_{\text{eff}}l\varepsilon, \qquad (16)$$

where n_{eff} represents the effective refractive index of the fiber core. For silica materials at wavelength λ = 1300 nm the parameters are $n = 1.46$, $\mu = 0.25$, $p_{11} \approx 0.12$, and $p_{12} \approx 0.27$,[13] and the effective index can be calculated as $n_{\text{eff}} \approx 1.19$.

Therefore the strain can be measured by

$$\varepsilon = \frac{\Delta x}{n_{\text{eff}}l}, \qquad (17)$$

and the combination specimen strain values were recorded by a resistance strain gauge indicator. The identical testing result is given by Fig. 6. Figure 7 shows the distribution strains measured by the various optical fiber sensors.

The accuracy of the measuring system is limited by the resolution of the scanning mirror, the smoothness of the fringe pattern profile, and the resolution of the center fringe identification. For this reason, in the present study we used a signal filter and a high-resolution stepper motor (1-μm step intervals) to scan the distance. Therefore the resolution of the
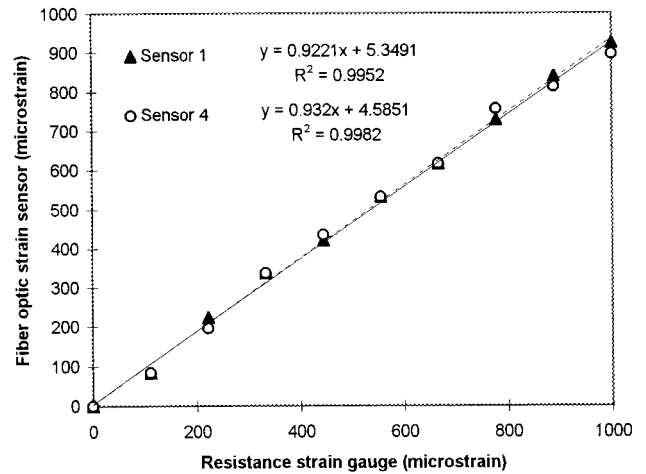

Fig. 6. Two fiber optic strain sensors identical attached at one point and with the same amount of stress applied to each sensor.

central fringe identification was ± 1 μm, and the identification repeatability of the central fringe was estimated as less than ± 1 fringe, which is equivalent to 0.6 μm for a 1300-nm LED source.[10] The procedure can be repeated for automatic measurements of successive strain sensing changes. The scanning time is ~10 s for each sensor, and the interval between scans can be adjusted from 1 s to many hours.

In fact, when the fiber optic sensors are embedded a material (such as epoxy, plastic, or concrete) in which the strain is to be measured, the deformation of the specimen (matrix material) will induce changes in the optical fiber, and this elongation of the fiber divided by the fiber gauge length and the effective refractive index can be measured as strain on the fiber itself. If the matrix–glass fiber bond is perfect, the two configurations will be equally sensitive to the imposed strain. That is, the strain in the glass fiber will be equal to the strain in the surrounding matrix. However, in practice, the fiber has a polymer coating and so is far less rigid than the glass fiber and the
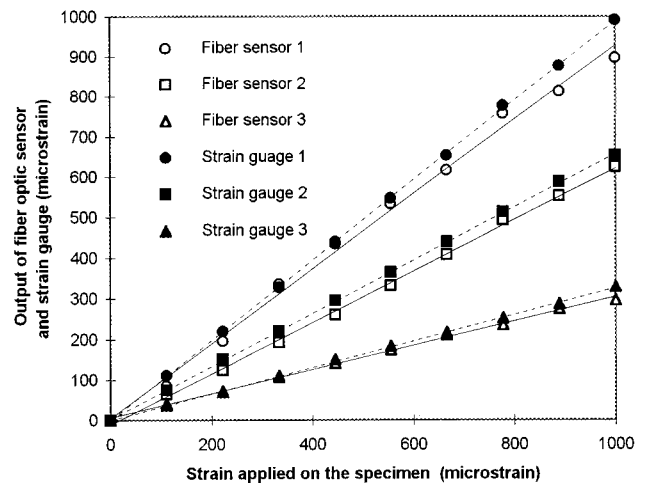

Fig. 7. Test results for various fiber optic strain sensors and strain gauges with various amounts of resistence.

surrounding matrix material. Therefore, even with a perfect matrix–fiber bond, the layered cross section is expected to affect the performance of the fiber sensor. It can be predicated that the strain measured by a length of fiber will be less than the real matrix strain. For all practical purposes, the strain measurements by the resistance strain gauge reflect the actual strains induced in the specimen. Then the strain values measured by fiber optic sensors should be smaller than the values measured by resistance strain gauges. This result is confirmed by our experiment as shown in Fig. 7.

6. Conclusions

When the unique compatibility of optical fiber sensors and composite structures is fully implemented to create smart structures, many benefits will be realized. Ideally, the simple and low-cost installation of fiber optic sensors will provide (1) a fabrication cure monitor; (2) a built-in sensor for testing suitability of components; (3) an in-service monitor for tracking structure response to characterize fatigue and to assess damage, and (4) a response feedback sensor for implementation of an active damping or control reconfiguration. Demonstrations reported here indicate that $1 \times N$ star coupler distribution strain fiber optic sensors in a white-light interferometer system may provide all these desirable sensing functions.

The system described herein provides a simple, potentially low-cost distribution strain-measurement method that will permit the use of commercial communication single-mode optical fibers as sensors in smart materials and structures as well the development of different gauge-length fiber optic strain sensors for a wide range of engineering applications.

References

1. A. S. Gerges, F. Farahi, T. P. Newson, J. D. C. Jones, and D. A. Jackson, "Fiber-optic interferometric sensor utilising low coherence length source-resolution enhancement," Electron. Lett. **24,** 472–474 (1988).
2. C. E. Lee and H. F. Taylor, "Fiber-optic Fabry–Perot temperature sensor using a low coherence light source," J. Lightwave Technol. **9,** 129–134 (1991).
3. Y. N. Ning, K. T. V. Grattan, and A. W. Palmer, "Fiber-optic interferometric system using low coherence light source," Sensors Actuators A **30,** 181–192 (1992).
4. B. R. Fogg and A. Wang, *Fiber Optic Sensor-Based Smart Materials and Structures* (Institute of Physics, Bristol, UK, 1992), p. 51.
5. L. Yuan, "White-light interferometric fiber-optic strain sensor from three-peak-wavelengths broadband LED source," Appl. Opt. **36,** 6246–6250 (1997).
6. Y. J. Rao and D. A. Jackson, "Long-distance fiber-optic white-light displacement sensing system using a source-synthesizing technique," Electron. Lett. **31,** 310–311 (1995).
7. V. Bhatia, K. A. Murphy, R. O. Claus, M. E. Jones, J. L. Grace, T. A. Tran, and J. A. Greene, "Optical fiber based absolute extrinsic Fabry–Perot interferometric sensing system," Meas. Sci. Technol. **7,** 58–62 (1996).
8. L. Yuan and F. Ansari, "White-light interferometric fiber-optic distributed strain-sensing system," Sensors Actuators A **63,** 177–181 (1997).
9. A. Koch and R. Ulrich, "Fiber-optic displacement sensor with 0.02 μm resolution by white-light interferometry," Sensors Actuators A **57,** 25–27 (1991).
10. T. Li, A. Wang, K. Murphy, and R. Claus, "White-light scanning fiber Michelson interferometer for absolute position-distance measurement," Opt. Lett. **20,** 785–787 (1995).
11. M. Born and E. Wolf, *Principles of Optics*, 6th ed. (Pergamon, Oxford, 1980), p. 246.
12. C. D. Butter and G. B. Hocker, "Fiber optics strain gauge," Appl. Opt. **17,** 2867–2869 (1978).
13. D. A. Pinnow, "Elastooptical materials," in *Handbook of Lasers*, R. J. Pressley, ed. (CRC Press, Cleveland, Ohio, 1971), pp. 116–129.
14. M. P. Roe, B. Wacogne, and C. N. Pannell, "High-efficiency all-fiber phase modulator using an annular zinc oxide piezoelectric transducer," IEEE Photon. Technol. Lett. **8,** 1026–1028 (1996).